

Article

An Anisotropic Hydrogel with Simple Preparation and Well-Defined Structure as a New Platform for Flexible Sensors with Directional Strain and Force Sensing

Yitong Xie^{1,2}, Shuxu Wang^{1,*}, Yunlei Zhang¹, Hayato Kanai¹, Kuniyo Yamada¹, Toshie Wakamatsu¹, Yuko Hamada¹, Sei Obuse¹, Daihui Zhang², Fuxiang Chu², and Yasuhiro Ishida^{1,*}

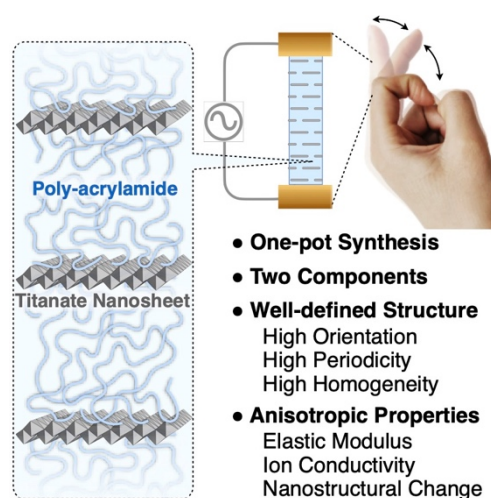
¹ RIKEN Center for Emergent Matter Science, 2-1 Hirosawa, Wako, Saitama 351-0198, Japan

² Institute of Chemical Industry of Forest Products, Chinese Academy of Forestry (CAF), No 16, Suojin Wucun, Nanjing 210042, China

* Correspondence: shuxu.wang@riken.jp (S.W.); y-ishida@riken.jp (Y.I.)

Received: 10 April 2025; Revised: 16 June 2025; Accepted: 18 June 2025; Published: 25 June 2025

Abstract: As a platform to construct the next-generation flexible strain and force sensors, anisotropic hydrogels have recently attracted considerable attention, with an expectation that they would visualize the anisotropic motion of biological systems in a direction-specific manner. To date, a number of anisotropic hydrogels have been developed with an intensive pursuit to improve their practical performance, so that their composition, preparation, and structure have become increasingly complex over the years. In fact, most of these anisotropic hydrogels are prepared from many components including naturally occurring materials, using multiple steps that often require skillful control of kinetic events. Therefore, although some of them show good performances, their complicated and unclear structures make it difficult to elucidate the relationship between structure and properties. As an approach complementary to such trend, here we report a very simple anisotropic hydrogel that would provide a versatile platform for flexible sensors with directional sensing capability. This hydrogel was simply prepared by one-pot reaction from two components, i.e., by magnetic orientation of titanate nanosheet (TiNS) in water and subsequent in-situ formation of a polyacrylamide network. In the resulting hydrogel (TiNS-gel), TiNS platelets were arranged in a lamellar structure with highly oriented, periodic, and homogeneous state. Due to such structure, TiNS-gel exhibited remarkable anisotropy in tensile modulus, nanostructural transformability, and ionic conductivity. Furthermore, TiNS-gel changed its electrical resistance upon tensile deformation, demonstrating its potential utility as a flexible strain and force sensor. TiNS-gel, characterized by easy synthesis, simple composition, well-defined structure, and various anisotropic properties will serve as a useful platform for developing flexible devices with direction-selective strain and force sensing capabilities.



Keywords: anisotropic hydrogels; nanosheets; magnetic alignment; strain sensing; force sensing; flexible electronics; wearable devices

1. Introduction

Hydrogels, a class of soft and flexible polymer networks that retain abundant water, have attracted considerable attention as attractive materials for constructing advanced devices [1–3]. Their inherent flexibility, tunable physical properties, and biocompatibility make hydrogels promising platforms for wearable electronics, soft robotics, and bio-integrated systems [4,5]. In fact, some hydrogels can conform to complex shapes, respond to external stimuli, and provide mechanical or electrical feedback, suggesting their potential use in flexible and



Copyright: © 2025 by the authors. This is an open access article under the terms and conditions of the Creative Commons Attribution (CC BY) license (<https://creativecommons.org/licenses/by/4.0/>).

Publisher's Note: Scilight stays neutral with regard to jurisdictional claims in published maps and institutional affiliations.

wearable devices. Compared to other soft elastomers, an additional advantage of hydrogels is their similarity to biological tissue [6,7], which allows for seamless integration with human skin or other soft interfaces, leading to various applications such as motion monitoring, pressure sensing, and dynamic force detection [8–10].

Traditionally, hydrogels with isotropic structures have been used for such flexible sensors [11,12], while recently, hydrogels with anisotropic structures and properties [13–20] have attracted considerable attention due to their potential to visualize anisotropic motion of biological systems in a direction-specific manner. For this aim, various anisotropic hydrogels have been developed in these years [21–37]. Some of them exhibit excellent sensing ability, such as high sensitivity [25,28], rapid sensing [24], repeatability [26,31,34], and strain–signal linearity [34]. Remarkable progress has also been made in mechanical properties, including enhanced modulus [23], stretchability [24,25], fracture strength [23,29] and fracture energy [33]. Additional functions have also been realized, including moisture-electric generation [21], self-healing [22,23], swelling resistance [26,30], photo responsiveness [35], and magnetothermal conversion [36]. Further advanced applications have also been pursued, including action signal prediction and classification driven by machine learning [27], and in vivo intraspinal neural recordings [31].

However, most of them have been designed with a focus on practical performance only, so that their preparations, compositions, and structures have become increasingly complex over the years. In fact, most of these anisotropic hydrogels are composed of three or more components, including biomass-derived materials (white wood [21–23], cellulose nanofiber [24], chitosan [24], sodium alginate [25,26], etc.) that tend to have different properties depending on their origin. In addition, these components are assembled through many steps that often require the skillful control of kinetic events (delignification [21–23], infiltration [21–23,27], spinning [24], pre-stretching [25–32], post metal chelation [25–30,32], salt out [33], directional ice growth [33,34], etc.). Consequently, the resulting hydrogels tend to have complex and ambiguous internal structures, whose structural anisotropy and uniformity are not always quantitatively evaluated. There may also be a potential risk in the quality control of such hydrogel samples, since their properties tend to depend on the purities of the plant-derived components and the skill of operators etc. Under such circumstances, even though some of them show good performance, their complicated and unclear structures make it difficult to elucidate the relationship between structures and properties.

To address this situation, here we report a very simple anisotropic hydrogel that can provide a versatile platform for the construction of flexible sensors with directional sensing ability. This hydrogel was obtained in a one-pot reaction from two components, i.e., by magnetic orientation of titanate nanosheets (TiNS) [38,39] in water and subsequent in-situ formation of a polyacrylamide network [13,40–44]. TiNS is a sort of monolayer single crystal of TiO₆ octahedra with a ultrathin (0.75-nm thickness) and ultrawide (several- μ m width) shape, and is magnetically orientable due to its anisotropic diamagnetic susceptibility [45,46]. The resulting gel (TiNS-gel) exhibited remarkable anisotropy in tensile modulus and ionic conductivity. As a mechanism of tensile anisotropy, the nanostructure of TiNS-gel was found to drastically change specifically in response to the stretching of the gel perpendicular to TiNS platelets. Furthermore, TiNS-gel changed its electrical resistance upon tensile deformation, demonstrating its potential utility as a flexible strain and force sensor. Given the clear relationship between its structure and properties, TiNS-gel is a useful platform for developing flexible devices with direction-selective strain and force sensing capabilities.

2. Materials and Methods

2.1. General

For deionization of aqueous dispersions of TiNS, a CF16RXII centrifuge equipped with a T15A41 rotor (Hitachi Koki, Tokyo, Japan) was used. For magnetic alignment of TiNS, a JMTD-10T100 superconducting magnet (Japan Superconductor Technology, Inc. (JASTEC), Kobe, Japan) with a bore of 100 mm was employed. Photoinduced radical polymerization was initiated with an OPM2-502H high-pressure mercury arc lamp (500 W) (USHIO, Tokyo, Japan). Small angle X-ray scattering (SAXS) measurements were conducted using a NANOPIX 3.5 m system equipped with a HyPix-6000 detector (Rigaku, Tokyo, Japan). Polarized optical microscopy (POM) images were taken using an Eclipse LV100POL optical polarizing microscope (Nikon, Tokyo, Japan). Mechanical tensile tests were performed using an ARES-G2 RW rheometer with a normal force sensor (TA Instruments, New Castle, DE, USA). Electrical resistance measurements were performed using a Keithley 2450 source meter (Tektronix, Beaverton, OR, USA).

Acrylamide (AAm) and *N,N'*-methylenebis(acrylamide) (BMAAm) were purchased from Tokyo Chemical Industry (TCI), Tokyo, Japan. Tetramethylammonium hydroxide (TMAOH; 15% water solution) and 2,2-diethoxyacetophenone (DEAP) were purchased from FUJIFILM Wako Pure Chemical, Osaka, Japan. The

commercially purchased reagents were used without purification. An aqueous dispersion of TiNS was synthesized according to the literature [38,39]. Deionized water was obtained from a Millipore Milli-Q integral water purification system (Merk Millipore, Burlington, MA, USA).

2.2. Preparation of TiNS-Gel

TiNS-gel was prepared by the procedure we reported previously [13,42]. Briefly, an aqueous dispersion of TiNS was deionized by repeating the cycle of centrifugation of TiNS dispersion, collection of TiNS sediment, and redispersion of TiNS sediment with deionized water 12 times [41]. The deionized aqueous dispersion of TiNS (0.6, 0.8, or 1.0 wt%) was mixed with TMAOH (0.3 mM), AAm (6.0 wt%), MBAAm (0.06 wt%), and DEAP (0.08 wt%) and then filled into a glass cell with 2 mm-thick. The cell was placed in the bore of a superconducting magnet with applying a 10 T magnetic field applied in the in-plane direction of the glass-sandwiched cell for 2.5 h. The cell was then irradiated with a mercury arc light for 2.5 h to afford a film of TiNS-gel. For each of the following experiments, the film was trimmed into rectangular strips of appropriate lengths and widths (e.g., 12 mm × 3 mm) so that the alignment of TiNS platelets became perpendicular and parallel to the sides of the rectangle (Figure S1).

2.3. SAXS Analysis

A strip of TiNS-gel was irradiated with an X-ray beam (CuK α , wavelength = 1.5418 Å) in the direction perpendicular to the film plane with the sample–detector distance of 1400 mm to collect a 2D scattering image, where the scattering vector q and the position of the incident X-ray beam were calibrated using the scattering image of silver behenate as a standard sample. The 2D scattering image was converted into the corresponding intensity– q plot and intensity–azimuthal angle plot using Fit2D software version 18 (<http://www.esrf.eu/computing/scientific/FIT2D/> (accessed on 1 July 2023)). For the intensity–azimuthal angle plot, the scattering intensity was integrated along the Debye-Scherrer ring with the q range of 0.1~1.0 nm⁻¹. For the SAXS measurement under tensile deformation of the gel, the relationship between the TiNS aligned direction and the stretched direction is shown in Figure 3.

2.4. Tensile Test

A strip of TiNS-gel was attached at its ends of the long axis with the sample stage and with the normal force sensor of a mechanical tester. With increasing the gap between the sample stage and the normal force sensor at a speed of 0.1 mm min⁻¹, the stress of the gel strip was recorded. The relationship between the alignment of TiNS platelets and the stretched direction is shown in the corresponding figures.

2.5. Evaluation of Strain/Force Sensing Ability

A strip of TiNS-gel was attached at its ends of the longer axis with copper wires, which connected to a source meter. The gel's ends were also attached to the sample stage and the normal force sensor of a mechanical tester. Upon increasing the gap between the sample stage and the normal force sensor at a speed of 0.1 mm min⁻¹, the electrical resistance and the stress of the gel strip were measured simultaneously. Alternatively, the gel strip connected to the source meter as above was pasted along the index finger with covering the second knuckle. Upon changing the bending angle of the knuckle among 0°, 45°, and 90°, the electrical resistance of the gel strip was measured. The resistance change ($\Delta R/R_0$) is defined as follows:

$$\Delta R/R_0 = (R - R_0)/R_0 \quad (1)$$

where R_0 and R were the initial resistance and resistance after sample stretching, respectively. The gauge factor (GF) and force sensitivity (FS), which are the indicators of the sensitivity of strain/force sensors, were calculated as follows:

$$GF = (\Delta R/R_0)/\Delta\varepsilon \quad (2)$$

$$FS = (\Delta R/R_0)/\Delta F \quad (3)$$

where $\Delta\varepsilon$ is the change in applied strain, while ΔF is the change in applied force.

3. Results and Discussion

3.1. Synthesis and Characterization of TiNS-Gel

Using the magnetic-alignment method as we have reported [13,42], films of TiNS-gel were synthesized (Figure 1a), where TiNS concentration was systematically changed (0.6, 0.8 and 1.0 wt%). 2D small-angle X-ray scattering (SAXS) measurements revealed a highly anisotropic and ordered arrangement of TiNS platelets in the gel. For example, TiNS-gel with [TiNS] = 0.8 wt% exhibited scattering specifically along the longitudinal direction as an array of regularly separated spots (Figure 1(bi)). Accordingly, the intensity–azimuthal angle plot obtained from the 2D scattering image showed two sharp peaks at 90° and 270° (Figure 1(bii)), indicating the alignment of TiNS platelets perpendicular to the magnetic field with an excellent order parameter of >0.95. In addition, the intensity– q plot obtained from the 2D scattering image showed a series of peaks corresponding to a layered structure of TiNS platelets with a uniform plane-to-plane distance of 35 nm (Figure 1(biii)). Such a large plane-to-plane distance, no less than 45 times larger than that of the thickness of a TiNS platelet, indicates the presence of strong electrostatic repulsion between them. Although the observation area of SAXS was limited by the size of the X-ray beam, polarized optical microscopy (POM) revealed that such a highly ordered arrangement of TiNS platelets was homogeneously present over a several centimeter size scale in the gel (Figure 1c). Overall, the combination of SAXS and POM analysis revealed the excellent structural anisotropy of TiNS-gel in a direct, quantitative, and global manner. This is in sharp contrast to the alignment evaluation of conventional anisotropic hydrogel sensors, which are usually based on the SEM images of gels after drying [21,24–29,31,33–36].

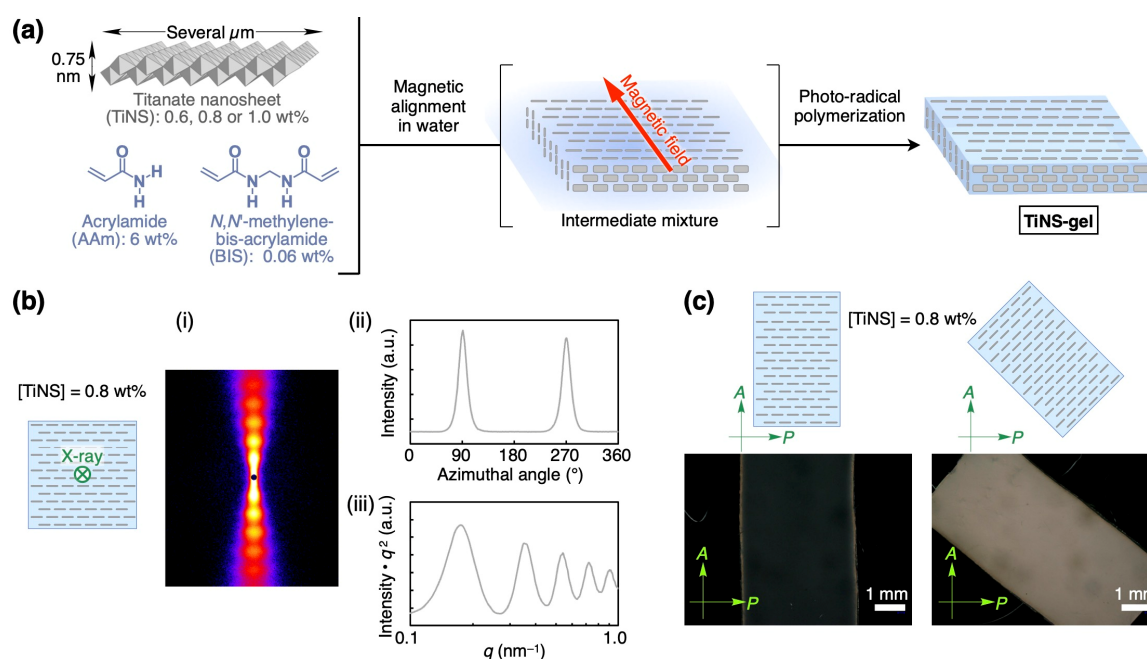


Figure 1. (a) Schematic illustration of the synthesis of TiNS-gel. (b) SAXS profiles of TiNS-gel: (i) 2D scattering pattern, (ii) intensity–azimuthal angle plot, and (iii) intensity– q plot. (c) POM images under crossed Nicols conditions of TiNS-gel with directing the alignment of TiNS platelets at angles of 0° (left) and 45° (right) relative to the polarizer. P and A denote the polarizer and analyzer, respectively.

Compared with other alignment methods such as shear-induced alignment and electric alignment, one attractive feature of magnetic alignment is its applicability to the alignment of thick samples due to the highly penetrative nature of magnetic fields. Another attractiveness of magnetic alignment is its high reproducibility. Indeed, multiple samples of TiNS-gel could be synthesized with good reproducibility, in terms of macroscopic homogeneity and microscopic anisotropy as confirmed by POM and SAXS (Figure S2). Although a drawback of the present method is that a 10 T magnetic field, which is not easily accessible in general, is indispensable for the alignment of diamagnetic TiNS, this problem would be addressed by using a ferromagnetic nanosheet $\text{Ti}_{0.8}\text{Co}_{0.2}\text{O}_2$ [47] in place of TiNS.

3.2. Mechanical Properties of TiNS-Gel

In our previous reports, the mechanical properties of TiNS-gel was investigated only in the compression of cubic samples for ease of operation [13,42]. Meanwhile, such compression is not very similar to the deformation that sensor films of flexible electronic devices undergo during their use. In addition, composite hydrogels such as TiNS-gel often exhibit quite different mechanical properties between compression and tensile deformation. Therefore, in the present work, we performed new tensile tests of TiNS-gel with stretching perpendicular and parallel to the alignment of TiNS platelets (Figure 2a). Regardless of the TiNS concentration, the modulus when stretched parallel to TiNS ($E_{//}$) was much higher than that when stretched perpendicular to TiNS (E_{\perp}) (Figure 2(ai–iii)). The anisotropic factor ($E_{//}/E_{\perp}$) was estimated to be 40–70, which manifests that TiNS-gel exhibits prominent mechanical anisotropy not only in compression as we reported previously [13,42] but also in tension. Also, the anisotropy factor of ~ 70 is at the top level among reported anisotropic hydrogels [19]. Reflecting on such direction-dependent hardness, the fracture strain ($^{\max}\varepsilon$) was also direction dependent. Thus, TiNS-gel with [TiNS] = 1.0 wt% was stretchable up to 6.5 times in the direction perpendicular to TiNS ($^{\max}\varepsilon_{\perp} = 550\%$) but was broken at 1.5 times upon parallel tensile ($^{\max}\varepsilon_{//} = 47\%$).

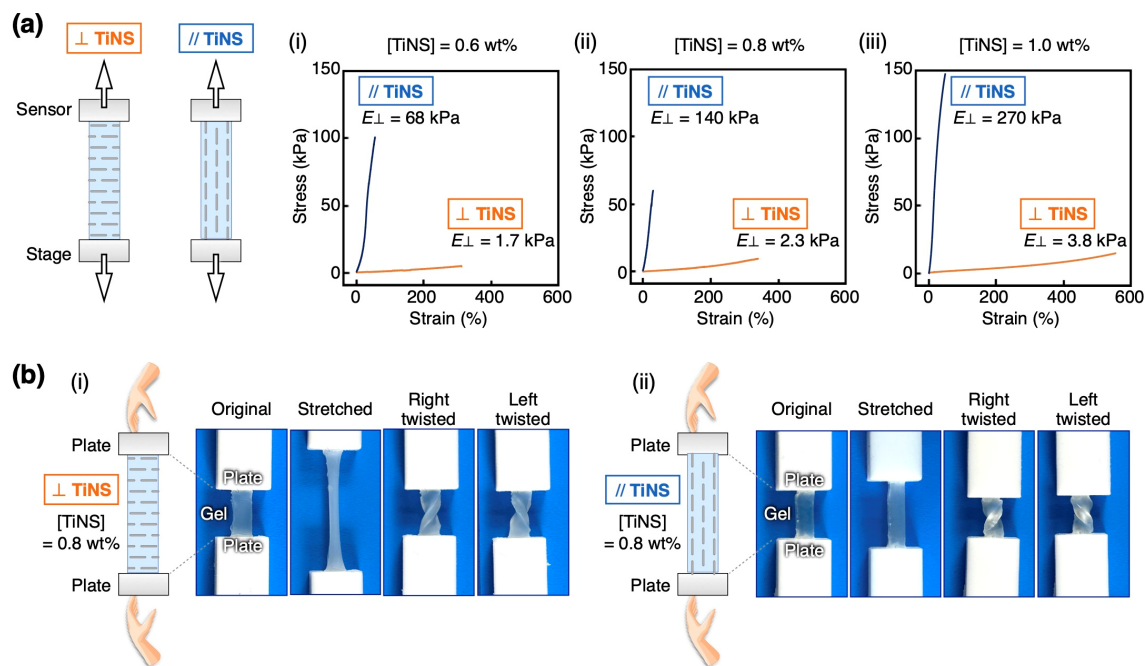


Figure 2. (a) Strain–stress curves of TiNS-gel upon tensile deformation along parallel (navy) and vertical (orange) to the alignment of TiNS platelets with TiNS concentrations of (i) 0.6, (ii) 0.8, and (iii) 1.0 wt%. (b) Optical images upon tensile and twist deformation of rectangular strips of TiNS-gel with TiNS platelets aligned (i) vertical and (ii) parallel to the longer axis of the rectangular shape.

In addition to the above uniaxial tensile test, a manual stretching and twisting of TiNS-gel could visualize its toughness and elasticity sufficient for application as strain/force sensors. Therefore, TiNS-gel was trimmed into rectangular strips with TiNS platelets aligned perpendicular (Figure 2(bi)) and parallel (Figure 2(bii)) to the long axis of the rectangle. The strips could be repeatedly stretched and twisted within the strain ranges blow their fracture points without notable crack formation and plastic deformation.

3.3. Mechanism for Tensile Anisotropy of TiNS-Gel though Nanostructure Change

To clarify the mechanism of the tensile anisotropy from the nanostructural viewpoints, TiNS-gel ([TiNS] = 0.8 wt%) was subjected to 2D SAXS measurement upon stretching perpendicular (Figure 3a) and parallel (Figure 3b) to the alignment of TiNS platelets. As described in the previous section, TiNS-gel before stretching exhibited a scattering pattern corresponding to the unidirectional orientation of TiNS platelets with a uniform plane-to-plane distance of 35 nm (Figure 3(ai–iii), original). However, when TiNS-gel was stretched in the direction perpendicular to TiNS platelet up to 25% strain, the scattering pattern changed to a more rounded shape with a shift toward the central region (Figure 3(ai), stretched), resulting in the broadening of the peaks in the intensity–azimuthal angle plot (Figure 3(aii), stretched) together with the broadening and smaller- q shift of the peaks in the intensity– q plot (Figure 3(aiii), stretched). Such changes indicate the orientational randomization of TiNS platelets [5] as well as the increase

and divergence of their plane-to-plane distance. Meanwhile, when the tensile force was released, the scattering profile became essentially similar to the original state (Figure 3(ai–iii), released), indicating the recovery of the original nanostructure. On the other hand, upon stretching parallel to TiNS platelets, the orientational order of TiNS platelets was hardly changed, while their plane-to-plane distance became narrower (Figure 3(bi–iii), stretched) [5]. When the tensile force was released, the plane-to-plane distance returned toward the original one (Figure 3(ai–iii), released). When the concentration of TiNS in the gel was varied between 0.6 and 1.0 wt%, essentially identical changes in the SAXS profiles upon tensile deformation were observed (Figures S3 and S4).

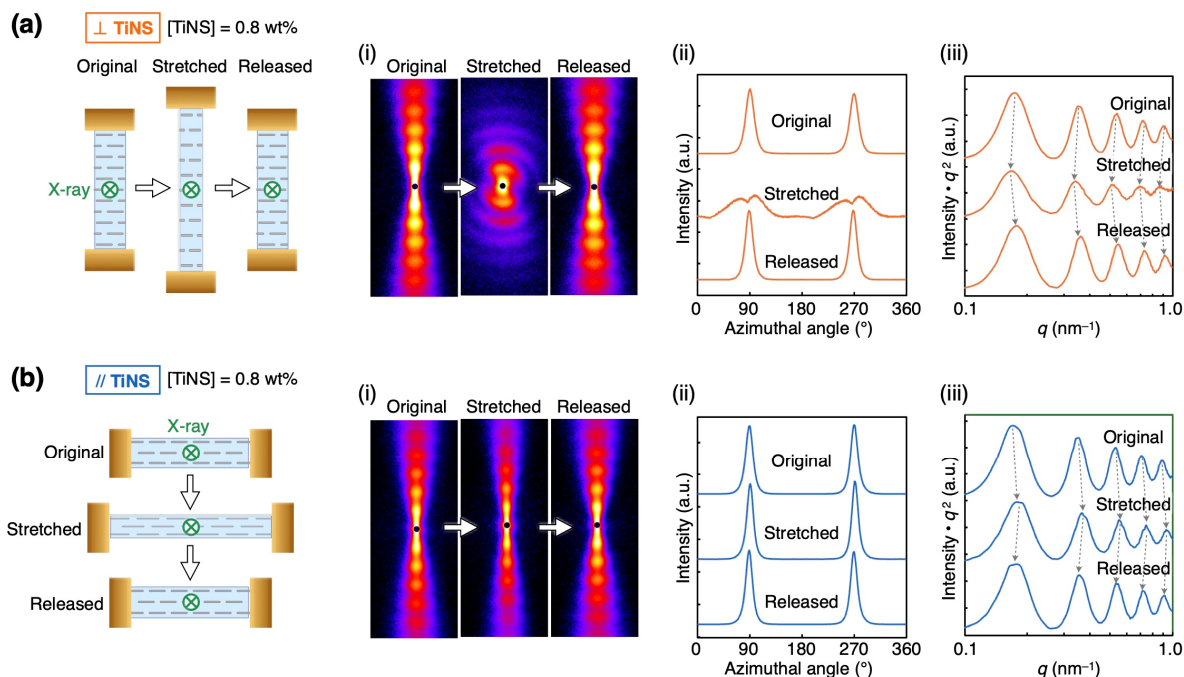


Figure 3. (a,b) Changes in the SAXS profiles of TiNS-gel ([TiNS] = 0.8 wt%) upon tensile deformation up to 25% strain along parallel (a) and vertical (b) to the alignment of TiNS platelets. Measurements were taken before deformation (original), after deformation (stretched), and then after releasing the force (released): (i) 2D SAXS images, (ii) intensity–azimuthal angle plots, and (iii) intensity– q plots.

Based on the nanostructural changes that occur upon tensile direction, as clarified above, the mechanism of the tensile anisotropy of TiNS-gel (Figure 2a) can be elucidated as follows. Upon parallel stretching (Figure 3b), the intrinsic hardness of TiNS platelets, the anchoring of polymer chains on TiNS platelets and the electrostatic repulsion between TiNS platelets are likely to cooperate to restrict the deformation of the gel, so that $E_{//}$ becomes high. In contrast, upon perpendicular stretching (Figure 3a), TiNS platelets are expected to buckle to lose their intrinsic hardness and polymer-anchoring ability, and to move away from each other to reduce the electrostatic repulsion, so that E_{\perp} becomes small.

The nanostructural changes described above imply that TiNS-gel has a certain durability upon tensile deformation. The original nanostructure was recovered when the tensile force was released, regardless of the direction (Figure 3). A more serious issue regarding long-term durability is the evaporation of water, a general problem with all hydrogels, not just TiNS-gel. When a film of TiNS-gel (10 mm × 10 mm × 2 mm) was placed in open air (25 °C, 50% RH) for 6 h, the film contracted preferentially in the direction perpendicular to the TiNS platelets due to water evaporation (Figure S5(ai)), and its weight decreased to 54% (Figure S5(aii)). The film contracted preferentially in the direction perpendicular to the TiNS platelets (Figure S5(ai)). During this drying process, the alignment of the TiNS platelets remained intact (Figure S5(bi)), while the periodic distance of the layered TiNS platelet structure decreased (Figure S5(bii)), consistent with the contraction of the entire film.

3.4. Ion Conductivity of TiNS-Gel

In our previous studies on TiNS-gel, its mechanical [13,42], actuation [40,43], and optical [41,44] properties have been extensively studied, while its electrical properties have never been explored. In the present work, we begin with evaluating the anisotropy in ion conductivity of TiNS-gel. At an alternating current (AC) mode, the resistance of TiNS-gel ([TiNS] = 0.8 wt%) was measured in the direction perpendicular and parallel to the alignment of TiNS platelets (Figure 4a). Over a frequency range of 0.1–10⁵ Hz, the resistance in the perpendicular

direction was one-order higher than that of the parallel direction (Figure 4(ai)). Furthermore, the phase difference also differs between the perpendicular and parallel measurements (Figure 4(aii)). These observations indicate that the ion migration parallel to TiNS platelets is smoother than the perpendicular one and that the capacitance parallel to TiNS platelets is larger than the perpendicular one.

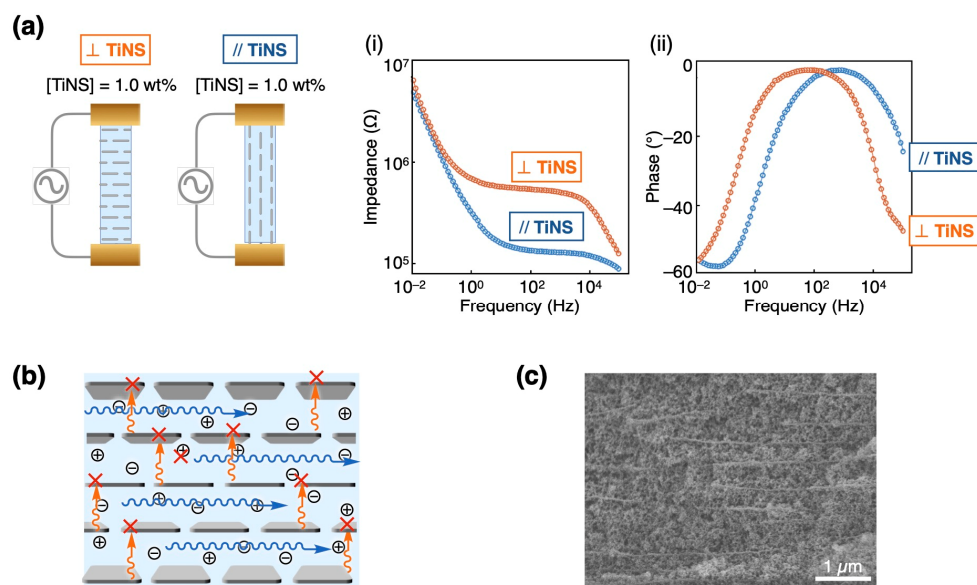


Figure 4. (a) Impedance–frequency (i) and phase–frequency (ii) curves of TiNS-gel measured along the direction parallel (navy) and vertical (orange) to TiNS. (b) Schematic illustration of ion transport in the anisotropic hydrogel. (c) Cross-sectional SEM image of the anisotropic hydrogel after fixation of the gel network and subsequent removal of water.

Such anisotropic resistance of TiNS-gel is attributable to the blocking of ion-migration by unidirectionally aligned TiNS platelets (Figure 4b,c). As depicted in the SAXS measurements (Figure 1b), TiNS platelets in TiNS-gel form a layered structure with a plane-to-plane distance of 35 nm. Given this structure, the ion-migration pathway is ensured in the direction parallel to TiNS platelets over a long range, while in the vertical direction, the pathway is intersected by TiNS platelets at each of the layer period. Although there exists a certain gap between neighboring TiNS platelets in same layer that would allow ions to migrate, the ratio of such gap relative to the whole area is negligibly small, as visualized by the scanning electron microscopy (SEM) cross-sectional image of the gel (Figure 4c), which was taken after fixation of the gel network by in-situ silica condensation and subsequent removal of water from the gel.

3.5. Resistance Change of TiNS-Gel upon Tensile Deformation

To evaluate the potential utility of TiNS-gel as a flexible strain sensor, we then investigated how TiNS-gel changes its electrical properties in response to the tensile deformation along perpendicular (Figure 5a) and parallel (Figure 5b) to the alignment of TiNS platelets, with resistance measured in the stretched direction. Upon perpendicular stretching of TiNS-gel ([TiNS] = 1.0 wt%) up to ~200% strain, the resistance change ($\Delta R/R_0$) raised to ~800% (Figure 5(ai)), demonstrating its sufficient sensitivity over a wide strain range. The resistance increased nonlinearly with strain, so that the gauge factor (GF_{\perp}) changed from 1.8 (0~50% strain) to 3.5 (60~110% strain) to 5.7 (120~160% strain). These GF values suggest that the sensitivity of the current system is moderate compared to other reported sensing systems based on anisotropic hydrogels [21–38]. This is probably because not only the macroscopic deformation of TiNS-gel but also the nanostructural change that occur upon perpendicular stretching, as clarified by our in-situ SAXS measurements (Figure 3a), contributed to the increase in resistance. The same tendency was observed regardless of the TiNS concentration in TiNS-gel (Figures S6 and S7).

Considering that the intrinsic ion conductivity of TiNS-gel is anisotropic (Figure 4) and that the nanostructure change of TiNS-gel occurs specifically depending on the tensile direction (Figure 3), the resistance change upon perpendicular stretching was expected to be different from that upon parallel stretching, which is favorable for directional strain sensing. However, the relationship between resistance change and tensile strain in parallel stretching differed only slightly from that in perpendicular stretching. The gauge factor of the parallel stretching (GF_{\parallel}) at 0~25% strain was 2.0 (Figure 5(bi)), which was only 1.1 times higher than that of the perpendicular

stretching at the similar strain range ($GF_{\perp} = 1.8$ at 0~50% strain; Figure 5(ai)). This unexpected result is likely because the anisotropy of resistance change is determined by the delicate balance of various anisotropic parameters. These parameters include not only ion conductivity and nanostructure change, but also macroscopic shape change, etc. [48,49]. Indeed, we confirmed that TiNS-gel exhibits a highly anisotropic Poisson's ratio upon stretching (Figure S8), which should also affect the anisotropy of resistance change. These anisotropic parameters do not always cooperate, but rather, they may compete to cancel their effects. In any case, to realize more directional strain sensing, further optimization is necessary, including the size of nanosheets, concentration, and components, as well as doping the gel with electron-conductive components. It should also be noted that, even for the latest flexible sensors based on anisotropic hydrogels, the anisotropy factors in GF are either undetermined [21,23–26,31,35] or moderate, ranging from 1.1 to 2.4 [22,27–30,32–34,36].

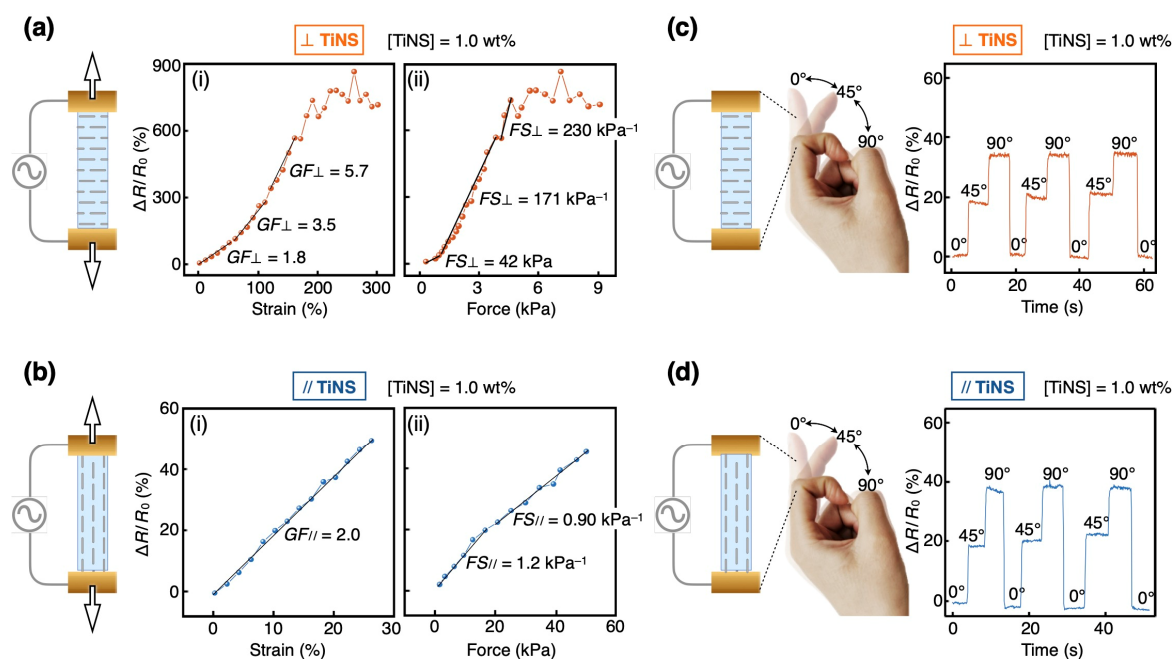


Figure 5. (a,b) Relative resistance change ($\Delta R/R_0$) of TiNS-gel ([TiNS] = 1.0 wt%) upon tensile deformation along parallel (a) and vertical (b) to the alignment of TiNS platelets: plots of (i) $\Delta R/R_0$ versus strain and (ii) $\Delta R/R_0$ versus force. (c,d) Application of TiNS-gel ([TiNS] = 1.0 wt%) as a strain/force sensors for monitoring the bending motion of a finger, with directing the alignment of TiNS platelets vertical (c) and parallel (d) to the finger.

Meanwhile, current TiNS-gel already seems to have a great potential as a direction-selective force sensor. Indeed, the resistance change–force plots (Figure 5(aii,bii)) reveal a critical difference in the force sensitivity (FS) between the perpendicular and parallel stretching, where FS of perpendicular stretching (Figure 5(aii); $FS_{\perp} = 42\sim 230 \text{ kPa}^{-1}$) was about two orders higher than that of TiNS-//gel (Figure 5(bii); $FS_{//} = 0.9\sim 1.2 \text{ kPa}^{-1}$). Such pronounced directional dependence of FS ($FS_{\perp} \gg FS_{//}$; Figure 5a,b) is attributable to the direction dependency of tensile elastic modulus ($E_{\perp} \ll E_{//}$; Figure 2a); because TiNS-gel is about 70 times easier to stretch in the perpendicular direction than in the parallel direction, and because the resistance in the stretched direction generally increases with increasing tensile strain, forces applied in the direction perpendicular to TiNS platelets are more sensitively reflected in the resistance change. These observations suggest that when TiNS-gel receives tensile forces in many directions, it would respond specifically to forces perpendicular to TiNS platelets.

Finally, as a preliminary attempt to assess the practical utility as flexible wearable sensors, we used TiNS-gel to monitor the binding motion of a finger. Thus, TiNS-gel ([TiNS] = 1.0 wt%) was trimmed into a rectangular strip (12 mm \times 3 mm) with the long axis of the rectangle perpendicular or parallel to the alignment of TiNS platelets (Figure S1), so that the gel strip was preferentially stretched along its long axis. The gel strip was pasted along the index finger with covering the second knuckle, and its resistance change ($\Delta R/R_0$) was monitored when the bending angle of the knuckle was changed among 0°, 45°, and 90° (Figure 5c,d). As a result, the bending and stretching motion of the finger could be monitored in real time with satisfactory sensitivity and low noise level over multiple cycles (Figure 5c,d).

4. Conclusions

We report an ultimately simple anisotropic hydrogel, which can be synthesized in a one-pot reaction from only two components. Despite its simple synthesis, our hydrogel possesses near-perfectly aligned structure and exhibits remarkable anisotropy in tensile modulus, nanostructural transformability, and ion conductivity, as well as strain/forces responsiveness in its electrical resistance. These observations suggest that our hydrogel will serve as a useful platform for the development of flexible devices with directional strain/force sensing capabilities. The clear structure–function relationship, which is a characteristic of our hydrogel compared with other anisotropic hydrogels developed for sensing applications, would provide new insight into anisotropy-driven mechanisms in soft sensing materials. Furthermore, this work would also contribute to theoretical elucidation of how nanoscopic structural orientation governs macroscopic sensing behavior, since the simple, well-defined, and near-perfectly anisotropic structure of this hydrogel is beneficial for theoretical modeling. Possible interesting challenges based on this hydrogel include the optimization of compositions to realize directional strain sensing, the introduction of electrically conductive components to improve sensitivity, and the introduction of photo-functional components for strain and force sensing by color change.

Supplementary Materials: The following supporting information can be downloaded at: https://media.sciltp.com/articles/others/2506251057370684/MI_882_SM-FC.pdf. Figure S1: Schematic illustration of the trimming of TiNS-gel into two types of rectangular strips; Figure S2: Reproducibility of TiNS-gel synthesis at 0.8 wt% was confirmed by SAXS and POM characterization of two additional batches; Figure S3: SAXS reveals anisotropic structural changes in TiNS-gel (0.6 wt%) under tensile strain along parallel and vertical directions; Figure S4: SAXS reveals anisotropic structural changes in TiNS-gel (1.0 wt%) under tensile strain along parallel and vertical directions; Figure S5: TiNS-gel (0.8 wt%) shows dimensional and structural changes during drying; Figure S6: Relationship between $\Delta R/R_0$ and applied tensile strain and force of TiNS-gel at [TiNS] = 0.6 wt%; Figure S7: Relationship between $\Delta R/R_0$ and applied tensile strain and force of TiNS-gel at [TiNS] = 0.8 wt%. Figure S8: TiNS-gel (0.8 wt%) exhibits different Poisson ratios depending on the tensile direction.

Author Contributions: Y.X., S.W. and Y.I. conceived the project. Y.X. and S.W. designed and performed all experiments. Y.Z. conducted the tensile measurements. K.Y., T.W., Y.H. and S.O. helped the preparation of TiNS-gel samples. H.K. conducted a part of SAXS measurements. Y.X., S.W., D.Z., F.C. and Y.I. analyzed the data and wrote the manuscript with the input of all other authors. All authors have read and agreed to the published version of the manuscript.

Funding: This work was supported by JST CREST Grant Number JPMJCR22B1.

Data Availability Statement: The data supporting this article have been included as part of the Supplementary Materials. Further data is available upon reasonable request from the authors.

Acknowledgments: We thank J. Liu (RIKEN) for SAXS measurements. Y. Xie acknowledges the Chinese Scholarship Council scholarship (No. 202303270021). S.W. acknowledges the Junior Research Associate (JRA) Program from RIKEN and JSPS for a Young Scientist Fellowship.

Conflicts of Interest: There are no conflict of interest to declare.

References

1. Zhang, Z.; Yang, J.; Wang, H.; Wang, C.; Gu, Y.; Xu, Y.; Lee, S.; Yokota, T.; Haick, H.; Someya, T.; et al. A 10-micrometer-thick nanomesh-reinforced gas-permeable hydrogel skin sensor for long-term electrophysiological monitoring. *Sci. Adv.* **2024**, *10*, eadj5389.
2. Li, Y.; Liu, C.; Zou, H.; Che, L.; Sun, P.; Yan, J.; Liu, W.; Xu, Z.; Yang, W.; Dong, L.; et al. Integrated wearable smart sensor system for real-time multi-parameter respiration health monitoring. *Cell Rep. Phys. Sci.* **2023**, *4*, 101191.
3. Xia, S.; Zhang, Q.; Song, S.; Duan, L.; Gao, G., Bioinspired dynamic cross-linking hydrogel sensors with skin-like strain and pressure sensing behaviors. *Chem. Mater.* **2019**, *31*, 9522–9531.
4. Gong, J., Double-network hydrogels with extremely high mechanical strength. *Adv. Mater.* **2003**, *15*, 1155–1158.
5. Wang, X.; Li, Z.; Wang, S.; Sano, K.; Sun, Z.; Shao, Z.; Takeishi, A.; Matsubara, S.; Okumura, D.; Sakai, N.; et al. Mechanical nonreciprocity in a uniform composite material. *Science* **2023**, *380*, 192–198.
6. Hu, L.; Chee, P.L.; Sugiarto, S.; Yu, Y.; Shi, C.; Yan, R.; Yao, Z.; Shi, X.; Zhi, J.; Kai, D.; et al. Hydrogel-based flexible electronics. *Adv. Mater.* **2023**, *35*, e2205326.
7. Gao, Q.; Sun, F.; Li, Y.; Li, L.; Liu, M.; Wang, S.; Wang, Y.; Li, T.; Liu, L.; Feng, S.; et al. Biological tissue-inspired ultrasoft, ultrathin, and mechanically enhanced microfiber composite hydrogel for flexible bioelectronics. *Nanomicro Lett.* **2023**, *15*, 139.
8. Bai, M.; Chen, Y.; Zhu, L.; Li, Y.; Ma, T.; Li, Y.; Qin, M.; Wang, W.; Cao, Y.; Xue, B., Bioinspired adaptive lipid-integrated bilayer coating for enhancing dynamic water retention in hydrogel-based flexible sensors. *Nat. Commun.* **2024**, *15*, 10569.
9. Park, B.; Shin, J.H.; Ok, J.; Park, S.; Jung, W.; Jeong, C.; Choy, S.; Jo, Y.J.; Kim, T.-i., Cuticular pad-inspired selective frequency damper for nearly dynamic noise-free bioelectronics. *Science* **2022**, *376*, 624–629.

10. Zhao, Z.; Liu, J.; Wu, M.; Yao, X.; Wang, H.; Liu, X.; He, Z.; Song, X., A soft, adhesive self-healing naked-eye strain/stress visualization patch. *Adv. Mater.* **2024**, *36*, e2307582.
11. Li, W.; Zheng, S.; Zou, X.; Ren, Y.; Liu, Z.; Peng, W.; Wang, X.; Liu, D.; Shen, Z.; Hu, Y.; et al. Tough hydrogels with isotropic and unprecedented crack propagation resistance. *Adv. Funct. Mater.* **2022**, *32*, 2207348.
12. Xie, Y.; Shi, X.; Gao, S.; Lai, C.; Lu, C.; Huang, Y.; Zhang, D.; Nie, S.; Xu, F.; Chu, F., Biomimicking natural wood to fabricate isotropically super-strong, tough, and transparent hydrogels for strain sensor and triboelectric nanogenerator applications. *J. Mater. Chem. A* **2024**, *12*, 5124–5132.
13. Liu, M.; Ishida, Y.; Ebina, Y.; Sasaki, T.; Hikima, T.; Takata, M.; Aida, T., An anisotropic hydrogel with electrostatic repulsion between cofacially aligned nanosheets. *Nature* **2015**, *517*, 68–72.
14. Mredha, M.T.I.; Guo, Y.Z.; Nonoyama, T.; Nakajima, T.; Kurokawa, T.; Gong, J.P., A facile method to fabricate anisotropic hydrogels with perfectly aligned hierarchical fibrous structures. *Adv. Mater.* **2018**, *30*, 1704937.
15. Hiratani, T.; Kose, O.; Hamad, W.Y.; MacLachlan, M.J. Stable and sensitive stimuli-responsive anisotropic hydrogels for sensing ionic strength and pressure. *Materials Horiz.* **2018**, *5*, 1076–1081.
16. Zhu, Q.L.; Du, C.; Dai, Y.; Daab, M.; Matejdes, M.; Breu, J.; Hong, W.; Zheng, Q.; Wu, Z.L. Light-steered locomotion of muscle-like hydrogel by self-coordinated shape change and friction modulation. *Nat. Commun.* **2020**, *11*, 5166.
17. Liang, X.; Chen, G.; Lin, S.; Zhang, J.; Wang, L.; Zhang, P.; Wang, Z.; Wang, Z.; Lan, Y.; Ge, Q.; et al. Anisotropically fatigue-resistant hydrogels. *Adv. Mater.* **2021**, *33*, e2102011.
18. Xue, P.; Bisoyi, H.K.; Chen, Y.; Zeng, H.; Yang, J.; Yang, X.; Lv, P.; Zhang, X.; Priimagi, A.; Wang, L.; et al. Near-infrared light-driven shape-morphing of programmable anisotropic hydrogels enabled by MXene nanosheets. *Angew. Chem. Int. Edition* **2021**, *60*, 3390–3396.
19. Sano, K.; Ishida, Y.; Aida, T., Synthesis of anisotropic hydrogels and their applications. *Angew. Chem. Int. Ed.* **2018**, *57*, 2532–2543.
20. Uchida, N.; Ishida, Y., Macroscopically oriented polymeric soft materials: Synthesis and functions. **2019**, *51*, 709–719.
21. Xiong, J.; Wu, W.; Hu, Y.; Guo, Z.; Wang, S., An anisotropic conductive hydrogel for strain sensing and breath detection. *Appl. Mater. Today* **2023**, *34*, 101909.
22. Zhang, Y.; Fu, Z.; Wu, T.; Ren, B.; Chen, J.; Xie, F.; Leng, W.; Shi, J.; Lu, Y., Skin-inspired ultra-tough, self-healing anisotropic wood-based electronic skin for multidimensional sensing. *Chem. Eng. J.* **2024**, *496*, 154000.
23. Teng, Y.; Zhang, Z.; Cui, Y.; Su, Z.; Godwin, M.; Chung, T.; Zhou, Y.; Leontowich, A.F.G.; Islam, M.S.; Tam, K.C.; et al. High-sensitivity and flexible motion sensing enabled by robust, self-healing wood-based anisotropic hydrogel composites. *Small* **2025**, *21*, 2500944.
24. Geng, L.; Liu, W.; Fan, B.; Wu, J.; Shi, S.; Huang, A.; Hu, J.; Peng, X., Anisotropic double-network hydrogels integrated superior performance of strength, toughness and conductivity for flexible multi-functional sensors. *Chem. Eng. J.* **2023**, *462*, 142226.
25. Chen, L.; Chang, X.; Chen, J.; Zhu, Y., Ultrastretchable, antifreezing, and high-performance strain sensor based on a muscle-inspired anisotropic conductive hydrogel for human motion monitoring and wireless transmission. *ACS Appl. Mater. Interfaces* **2022**, *14*, 43833–43843.
26. Zhang, Y.; Jing, X.; Zou, J.; Feng, P.; Wang, G.; Zeng, J.; Lin, L.; Liu, Y.; Mi, H.; Nie, S., Mechanically robust and anti-swelling anisotropic conductive hydrogel with fluorescence for multifunctional sensing. *Adv. Funct. Mater.* **2024**, *34*, 2410698.
27. Hang, C.; Guo, Z.; Li, K.; Yao, J.; Shi, H.; Ge, R.; Liang, J.; Quan, F.; Zhang, K.; Tian, X.; et al. Anisotropic hydrogel sensors with muscle-like structures based on high-absorbent alginate fibers. *Carbohydr. Polym.* **2025**, *349*, 123015.
28. Wang, W.; Deng, X.; Luo, C., Anisotropic hydrogels with high-sensitivity and self-adhesion for wearable sensors. *J. Mater. Chem. C* **2023**, *11*, 196–203.
29. Lin, H.; Wang, R.; Xu, S.; Li, X.; Song, S., Tendon-inspired anisotropic hydrogels with excellent mechanical properties for strain sensors. *Langmuir* **2023**, *39*, 6069–6077.
30. Ghosh, A.; Pandit, S.; Kumar, S.; Pradhan, D.; Das, R.K., Human muscle inspired anisotropic and dynamic metal ion-coordinated mechanically robust, stretchable and swelling-resistant hydrogels for underwater motion sensing and flexible supercapacitor application. *ACS Appl. Mater. Interfaces* **2024**, *16*, 62743–62761.
31. Huang, S.; Xiao, R.; Lin, S.; Wu, Z.; Lin, C.; Jang, G.; Hong, E.; Gupta, S.; Lu, F.; Chen, B.; et al. Anisotropic hydrogel microelectrodes for intraspinal neural recordings in vivo. *Nat. Commun.* **2025**, *16*, 1127.
32. Lin, H.; Yuan, W.; Zhang, W.; Dai, R.; Zhang, T.; Li, Y.; Ma, S.; Song, S., Strong and tough anisotropic short-chain chitosan-based hydrogels with optimized sensing properties for flexible strain sensors. *Carbohydr. Polym.* **2025**, *348*, 122781.
33. Fu, X.; Tong, H.; Zhang, X.; Zhang, K.; Douadji, L.; Kang, S.; Luo, J.; Pan, Z.; Lu, W., Anisotropic hydrogels with multiscale hierarchy based on ionic conductivity for flexible sensors. *ACS Appl. Polym. Mater.* **2023**, *5*, 9876–9887.
34. Chen, S.; Guo, B.; Yu, J.; Yan, Z.; Liu, R.; Yu, C.; Zhao, Z.; Zhang, H.; Yao, F.; Li, J., A polypyrrole-

- dopamine/poly(vinyl alcohol) anisotropic hydrogel for strain sensor and bioelectrodes. *Chem. Eng. J.* **2024**, 486, 150182.
35. Shang, M.; Ma, S.; Ma, J.; Guo, L.; Liu, C.; Xu, X., Somatosensory actuators based on light-responsive anisotropic hydrogel for storage encryption of information systems. *Chem. Eng. J.* **2024**, 496, 153895.
 36. Zhanga, X.; Langb, B.; Yu, W.; Jia, L.; Zhu, F.; Xue, Y.; Wu, X.; Qin, Y.; Chen, W.; Wang, Y.; et al. Magnetically induced anisotropic conductive hydrogels for multidimensional strain sensing and magnetothermal physiotherapy. *Chem. Eng. J.* **2023**, 474, 145832.
 37. Chen, Z.; Wang, H.; Cao, Y.; Chen, Y.; Akkus, O.; Liu, H.; Cao, C., Bio-inspired anisotropic hydrogels and their applications in soft actuators and robots. *Matter* **2023**, 6, 3803–3837.
 38. Sasaki, T.; Watanabe, M.; Hashizume, H.; Yamada, H.; Nakazawa, H. Macromolecule-like aspects for a colloidal suspension of an exfoliated titanate. Pairwise association of nanosheets and dynamic reassembling process initiated from it. *J. Am. Chem. Soc.* **1996**, 118, 8329–8335.
 39. Tanaka, T.; Ebina, Y.; Takada, K.; Kurashima, K.; Sasaki, T., Oversized titania nanosheet crystallites derived from flux-grown layered titanate single crystals. *Chem. Mater.* **2003**, 15, 3564–3568.
 40. Kim, Y.S.; Liu, M.; Ishida, Y.; Ebina, Y.; Osada, M.; Sasaki, T.; Hikima, T.; Takata, M.; Aida, T., Thermoresponsive actuation enabled by permittivity switching in an electrostatically anisotropic hydrogel. *Nat. Mater.* **2015**, 14, 1002–1007.
 41. Sano, K.; Kim, Y.S.; Ishida, Y.; Ebina, Y.; Sasaki, T.; Hikima, H.; Aida, T. Photonic water dynamically responsive to external stimuli. *Nat. Commun.* **2016**, 7, 12559.
 42. Sano, K.; Arazoe, Y.; Ishida, Y.; Ebina, Y.; Osada, M.; Sasaki, T.; Hikima, T.; Aida, T., Extra-large mechanical anisotropy of a hydrogel with maximized electrostatic repulsion. *Angew. Chem. Int. Ed.* **2018**, 57, 12508–12513.
 43. Sun, Z.; Yamauchi, Y.; Araoka, F.; Kim, Y.S.; Bergueiro, J.; Ishida, Y.; Ebina, Y.; Sasaki, T.; Hikima, T.; Aida, T., An Anisotropic hydrogel actuator enabling earthworm-like directed peristaltic crawling. *Angew. Chem. Int. Ed.* **2018**, 57, 15772–15776.
 44. Zhan, Y.; Ogawa, D.; Sano, K.; Wang, X.; Araoka, F.; Sakai, N.; Sasaki, T.; Ishida, Y., Reconfigurable photonic crystal reversibly exhibiting single and double structural colors. *Angew. Chem. Int. Ed.* **2023**, 62, e202311451.
 45. Gabriel, J.-C. P.; Camerel, F.; Lemaire, B.J.; Desvieux, H.; Davidson, P.; Batail, P. Swollen liquid-crystalline lamellar phase based on extended solid-like sheets. *Nature* **2001**, 413, 504–508.
 46. Hu, H.; Gopinadhan, M.; Osuji, C.O., Directed self-assembly of block copolymers: A tutorial review of strategies for enabling nanotechnology with soft matter. *Soft Matter* **2014**, 10, 3867–3889.
 47. Osada, M.; Ebina, Y.; Fukuda, K.; Ono, K.; Takada, K.; Yamaura, K.; Takayama-Muromachi, E.; Sasaki, T., Ferromagnetism in two-dimensional $\text{Ti}_{0.8}\text{Co}_{0.2}\text{O}_2$ nanosheets. *Phys. Rev. B* **2006**, 73, 153301.
 48. Qu, M.; Xie, Z.; Liu, S.; Zhang, J.; Peng, S.; Li, Z.; Lin, C.; Nilsson, F., Electric resistance of elastic strain sensors—Fundamental mechanisms and experimental validation. *Nanomaterials* **2023**, 13, 1813.
 49. Vázquez-Torres, N.A.; Benítez-Martínez, J.A.; Vélez-Cordero, J.R.; Sánchez-Arévalo, F.M., Experimental and numerical characterization of a flexible strain sensor based on polydimethylsiloxane polymeric network and MWCNT's. *J. Polym. Res.* **2024**, 31, 211.